Synthesis and Gas Sensing Performance of Dandelion-Like ZnO with Hierarchical Porous Structure

Faying Fan, Yongjun Feng, Pinggui Tang, Aifan Chen, Ruixian Luo, and Dianqing Li*

State Key Laboratory of Chemical Resource Engineering, Beijing University of Chemical Technology, Beijing 100029, China

Ⓢ Supporting Information

ABSTRACT: It is of great interest to develop gas-sensing materials with excellent performance in a facile and mild route. In this work, dandelion-like hollow ZnO hierarchitectures assembled with ZnO nanoparticles have been synthesized by annealing a zinc complex precursor, which was produced from zinc acetate and ammonium bicarbonate at room temperature. The nanoparticle size in the hierarchitectures enlarges from 10 to 23 nm with the annealing temperature increasing from 350 to 550 °C. The ZnO hierarchitectures have shown high sensing response (34.5), fast response (6 s) and recovery (7 s), and low optimal operating temperature (250 °C) toward 50 ppm ethanol because of large surface area and rich pore. Also, the obtained ZnO dandelion-like hierarchitectures exhibits good selectivity toward alcohols. The obtained results suggest that the dandelion-like ZnO hierarchitectures synthesized herein are a promising gas sensing material.

1. INTRODUCTION

In recent years, enormous efforts have been devoted to controllable construction of nanoscale building blocks (nanoparticles, nanorods, nanowires, and nanosheets) into desired hierarchical structures.[1,2] Such new structures can retain the properties of the individual building blocks and may further bring novel collective and cooperative properties.[3] For example, Tao et al.[4] prepared nanoparticle-based In-doped ZnO sphere aggregates which exhibit improved dye-sensitized solar cells conversion efficiency. Lou et al.[5] demonstrated that the SnO₂ tubular hierarchitectures composed by nanosheets show high specific capacity and excellent cycling stability. Specially, designed hierarchitectures constructed with nanoparticles are of great interest for researchers, because nanoparticles have the unique properties different from one-dimensional (1D) and two-dimensional (2D) nanomaterials resulting from their small size and higher specific surface area.[6] However, most of those reported hierarchitectures constructed with nanoparticles are sphere, nanorod, nanotube, and nanosheets;[7−10] the novel three-dimensional (3D) hierarchitectures composed by nanoparticles have rarely been reported.

Growing concern about air pollution with respect to public health has enhanced the demand for gas sensors for monitoring air quality. ZnO-based gas sensors have attracted great attention because of their high chemical stability and low toxity and cost. The sensing performance of the material is strongly dependent on their structures and morphology.[11−13] The ZnO nanomaterials with various dimensions have been widely studied in gas sensors, such as nanoparticles,[14] nanowires and nanorods,[13,15,16] nanoplates or nanosheets,[17] and 3D hierarchitectures.[18,19] Compared with low dimensional structures, 3D hierarchical structures possess large specific surface area and desirable surface permeability, which allows fast diffusion for target gases to interact with the entire sensing layer. Thus, both high sensing response and fast response could be expected by hierarchical structures. Kim et al.[20] pointed out that hierarchical structure played an important role in the fast

response to C₂H₅OH. Also, those materials assembled by nanoparticles have porous structures, which will provide high specific surface area and numerous connective channels. Therefore, it is an important issue to prepare ZnO 3D hierarchitectures assembled by nanoparticles with enhanced gas sensing properties.

Usually, metal oxide hierarchitectures with nanoparticles are prepared by hydro/solvothermal reaction, electrospinning, and vapor phase growth with high temperature, long reaction time, complicated procedure, and sometimes poisonous reagents.[6,21−24] It is still a great challenge to develop a facile and efficient method to produce ZnO hierarchitectures self-assembled with nanoparticles. Zinc oxide hierarchitectures prepared by thermal treatment of the precursor of basic carbonates,[25,26] ZnC₂O₄,[27] Zn(OH)₂,[28] carboxylate,[29,30] etc., have been reported, and such a method will provide ZnO with the novel morphology which inherit from the precursor. In this work, we fabricated dandelion-like ZnO hierarchitectures composed by nanoparticles with different diameters by thermal treatment of dandelion-like precursor of a zinc complex. Furthermore, we investigated the gas-sensing properties of the dandelion-like hierarchitectures using ethanol as the probe molecule and discussed the relationship between the structure and the gas-sensing performance of the ZnO hierarchitectures.

2. EXPERIMENTAL SECTION

2.1. Synthesis of the Precursor. All reagents were analytical grade and used without any further purification. NH₄HCO₃ (0.05 M, 3.95 g) and SDBS (2.5 mM, 0.8712 g) were dissolved in 100 mL of deionized water under vigorous stirring to form solution A; zinc acetate dihydrate (0.025 M, 5.4875 g) was dissolved in 25 mL of deionized water to form

solution B. Solution B was then added dropwise into solution A under stirring at 24 ± 1 °C and continuously stirred for 2 h. The precursor was collected after centrifugation, washed with deionized water and ethanol four times, and dried in an oven at 80 °C overnight.

2.2. Preparation of ZnO Hierarchitectures. The dandelion-like ZnO hierarchitectures composed of nanoparticles were obtained by annealing the precursor at 350, 450, and 550 °C in air for 2 h with a heating rate of 5 °C min^{-1}, which were marked as ZnO-350, ZnO-450, and ZnO-550, respectively.

For comparison, flower-like ZnO hierarchitectures composed of nanorods were also prepared by a hydrothermal method.[15] Briefly, solution A was prepared by dissolving 0.182 g of cetyltrimethylammonium bromide (CTAB) and 4.80 g of NaOH in 50 mL of deionized water; solution B was obtained by dissolving 5.95 g of zinc nitrate in 50 mL of deionized water. Solutions A and B were separately cooled in ice water for a few minutes and then mixed under vigorous stirring for 1 h at room temperature to form solution C. The resulting solution C was transferred into a 100 mL Teflon-lined autoclave and subsequently heated at 90 °C for 5 h. White ZnO product was obtained after washing and drying.

2.3. Characterization Methods. Powder X-ray diffraction patterns were recorded on a Rigaku D/max-Ultima III X-ray powder diffractometer with Ni-filtered Cu Kα radiation (λ = 0.15406 nm) under 45 kV and 40 mA with a scan speed of 5° per min in 2θ. The morphology of samples was examined using a scanning electron microscope (SEM ZEISS) with 20 kV accelerating voltage. The size distribution of ZnO samples was determined using high resolution transmission electron microscopy (HRTEM, JEM-3010) with a resolution of 0.19 nm. TEM images were recorded with Hitschi H-800. BET surface area and pore properties of ZnO samples were analyzed by low temperature N_2 adsorption/desorption method on a Micromeritics ASAP 2390 volumetric adsorption analyzer (before the BET measurement, the samples were degassed at 150 °C for 8 h).

2.4. Measurements of Gas Sensing Properties. The fabrication process of the sensors based on the samples has been reported elsewhere.[31] The dandelion-like ZnO and the reference ZnO samples were dispersed in ethanol to form colloid, and the colloid was separately coated on ceramic tube with a pair of previously printed electrodes. A Ni−Cr alloy was inserted into the ceramic tube and used as a heater to provide the operating temperature. The gas sensors were aged at 200 °C for 7 days before the gas sensing measurement. Gas sensing properties were measured by a CGS-8 intelligent gas sensing analysis system (Elite Tech Co., Ltd.). A schematic diagram of analysis system and experimental process were illustrated in the previous report.[32] The sensing response of oxidizing gases, such as NO_2, is defined as the ratio of R_a/R_g and the resistance for reducing gases, such as H_2, H_2S, alcohol, CH_4, CO, etc., are defined as the ratio of R_g/R_a, where R_a represents the resistance in ambient air and R_g is the resistance in the tested gas atmosphere.

3. RESULTS AND DISCUSSION

3.1. Structure and Morphology of ZnO Hierarchitectures. Figure 1 shows powder X-ray diffraction (PXRD) patterns of ZnO hierarchitectures and precursor (in the inset graph). All the samples obtained by annealing the precursor at 350, 450, and 550 °C are ZnO phase with hexagonal structure,
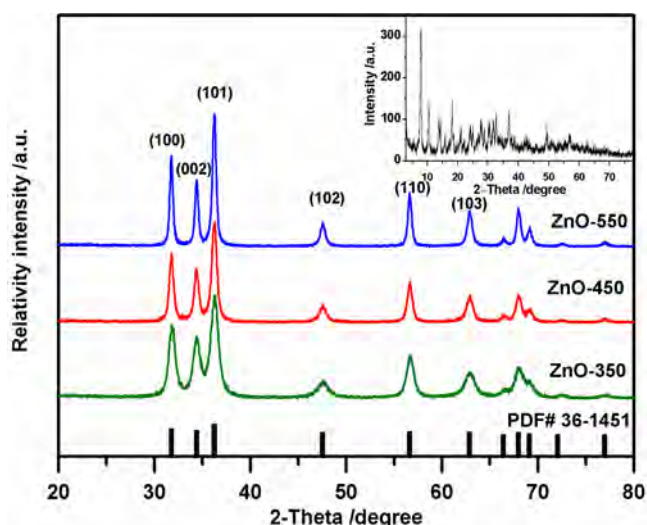

Figure 1. Powder X-ray diffraction (PXRD) patterns of ZnO-350, ZnO-450, and ZnO-550, respectively. Inset shows the PXRD patterns of the precursor. Vertical lines on the bottom represent JCPDS PDF card no. 36-1451 for hexagonal ZnO.

which well match with JCPDS PDF card no. 36-1451 as marked in the bottom of Figure 1. No diffraction peak of impurities is detected under the investigated conditions. In comparison, the intensities of the diffraction peaks gradually enhance with the increase of annealing temperature from 350 to 550 °C, indicating the increase of the crystallite size and the improvement of the crystallinity. The average crystallite size estimated based on Scherrer equation and the first three Bragg reflections is 9.93, 14.83, and 21.1 nm in diameter for ZnO-350, ZnO-450, and ZnO-550, respectively. For the precursor, the Bragg reflections peaks cannot be indexed to any known phase containing a zinc element. To further characterize the composition of precursor, Fourier transform infrared spectroscopy (FT-IR) was carried out. As shown in Figure S1, bands observed in the range of 3400−3600 cm^{-1} are indexed to hydroxyl groups and water, and two bands at 2927 and 2850 cm^{-1} are corresponded to C−H stretching vibration of −CH_2− for SDBS. The strong bands centered at 1546 and 1391 cm^{-1} are ascribed to the asymmetric and symmetric vibration of C═O, indicating that acetate was present in the complex.[33] The bands centered at 1046 and 834 cm^{-1} are assigned to the symmetric and out-of-plane stretches of CO_3^{2-} group, respectively.[17,34] FT-IR analyses confirm the precursor is a zinc complex containing carbonate, hydroxide groups, acetate, SDBS, and water.

Figure 2 demonstrates the SEM images of the precursor and the ZnO hierarchitectures with different magnification. The obtained precursor exhibits well-defined dandelion-like microspheres with a diameter of 3−8 μm (Figure 2A,B). The dandelion-like precursor is consisting of nanorods which are perpendicular to the microsphere surface to form open-ended structure (Figure 2B). The precursor has converted to the hexagonal ZnO by annealing at 350 °C in air for 2 h, while the morphology still remains dandelion-like without any change in size, as shown in Figure 2C,D. Interestingly, the inset graph for the cracked microsphere shows a hollow structure formed by closely well-aligned aggregating of these nanorods. Figure 2E,F present the SEM images of ZnO-450 and ZnO-550. It is clearly shown that higher annealing temperature did not lead to much
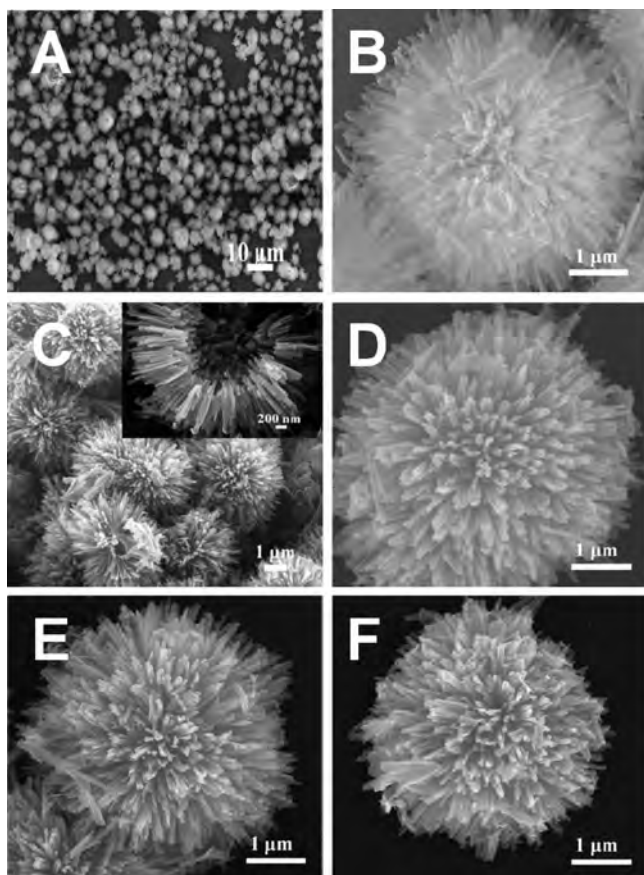
Figure 2. SEM images of the samples: precursor (A and B), ZnO-350 (C and D), ZnO-450 (E), and ZnO-550 (F); the inset in C presents a hollow structure of the ZnO-350.
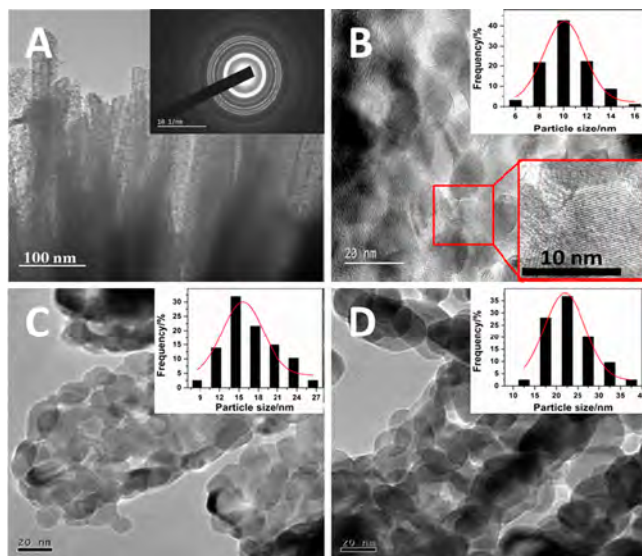

Figure 3. TEM and HRTEM images of dandelion-like ZnO hierarchitectures: ZnO-350 (A and B), ZnO-450 (C), and ZnO-550 (D); inset in A is the SAED pattern of ZnO-350; insets in B are the size distribution of nanoparticles for ZnO-350 (up-right) and magnified views of the areas marked by dotted squares (down-right); insets in C and D are size distribution for ZnO-450 and ZnO-550, respectively.
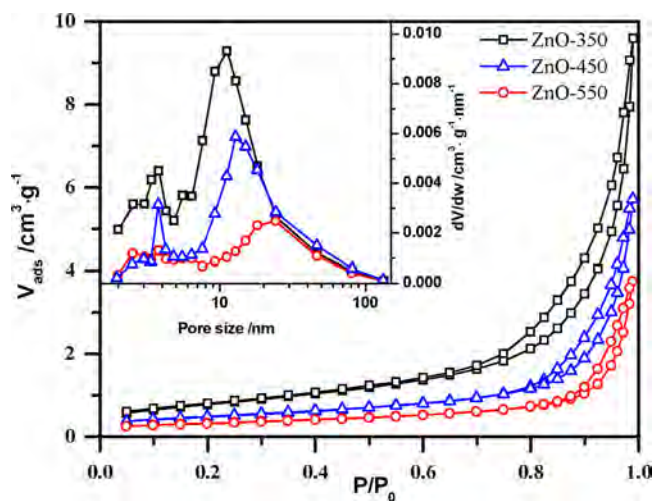

Figure 4. Nitrogen adsorption−desorption isotherms and pore size distribution curves of dandelion-like ZnO hierarchitectures.

change of morphology and size, while the outlines of nanorods are clearer.

Figure 3 shows the TEM and HRTEM images of the ZnO hierarchitectures. Figure 3A clearly shows that these nanorods of hierarchitectures are composed of plenty of tiny nanoparticles. Also, the diameter and length of these nanorods are in the ranges of 40−80 nm and 0.8−1.5 μm, respectively. Figure 3B indicates that each nanoparticles exhibits well-defined lattice fringes, and the inset displays the size distribution of the nanoparticle building blocks of ZnO-350 dandelion-like hierarchitectures. It shows that the average diameter of these nanoparticles is 10 ± 4 nm. Figure 3C,D illustrates the HRTEM images and size distribution of ZnO-450 and ZnO-550. The results indicate that the increases of annealing temperature enlarges the average particle size from 10.0 nm for ZnO-350 to 16.7 nm for ZnO-450 (Figure 3C) and 23.2 nm for ZnO-550 (Figure 3D).

Figure 4 describes the nitrogen adsorption−desorption isothermal curves for ZnO-350, ZnO-450, and ZnO-550. The hysteresis features of all the samples belong to type H3 loop, which does not show any limiting adsorption at high P/P_0, suggesting the presence of slit-shaped pores formed by aggregation of particles.[35] The following abrupt increase in the curves at high relative pressure, P/P_0 of about 0.95, can be ascribed to the capillary condensation of nitrogen in the macropores formed among the resultant nanoparticles.[36,37] The BET surface areas of as-synthesized porous dandelion-like hierarchitectures are 63.4, 38.76, and 25.77 $m^2 \cdot g^{-1}$ for ZnO-

350, ZnO-450, and ZnO-550, respectively. The pore size distribution curves as shown in the inset show that all samples of the ZnO dandelion-like hierarchitectures have a bimodal pore distribution, smaller pores in the range of 1−5 nm and the larger pores ranging from 6 to 100 nm. The average pore size of hierarchitectures is 14.73, 18.24, and 22.85 nm for ZnO-350, ZnO-450, and ZnO-550, respectively. The increase of larger pore size with the increase of annealing temperatures can be ascribed to the sintering of the small nanoparticles.

3.2. Gas-Sensing Performance of ZnO Samples. The performance of the sensors includes the sensing response, operating temperature, selectivity, the linear response range, and the response-recovery time, which depend on the properties of the gas-sensing materials. Also, flower-like ZnO hierarchitectures fabricated by 1-D nanorods with single crystal

were used as the reference, which was prepared following the same procedure in our previous work.[15] The morphology and structures of the obtained 1-D nanorods are presented in Figure S2. It indicates that the compared ZnO is single crystal with flower-like structure. Here, all four gas-sensing materials were individually fabricated to gas sensors, and then the gas sensing performance of the prepared sensors was detected.

Figure 5 displays the sensing response of the ZnO samples toward 50 ppm ethanol as a function of operating temperatures.
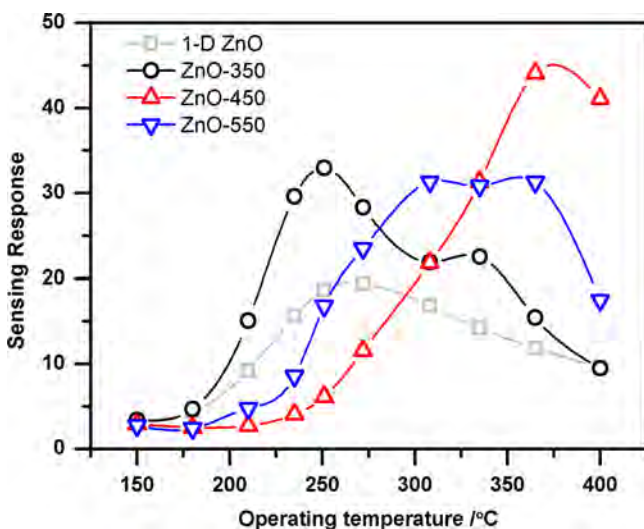

Figure 5. ZnO gas sensors response to 50 ppm ethanol under different operating temperature.

The sensing response increases and then decreases in the range of the operation temperature from 150 to 400 °C. It is well-known that the gas sensing properties of semiconductor material involves the adsorption and desorption of gases and reaction of the adsorbed gases on the surface-active sites of the material.[38] Sufficient thermal energy is essential to overcome the activation energy barrier for chemisorption and reaction between adsorbed gases on the surface of material. The amount of chemical-adsorbed gas molecules increases with the increase of operating temperature, and the higher sensing response is obtained.[39] However, as the operating temperature further increases, the desorption process becomes dominant, resulting in the decrease of the response.[40−43] Therefore, the sensing response will increase first and then decreases with the increasing of operating temperature. The optimum operating temperature at which the response reaches the highest value is ca. 250, 370, and 330 °C for ZnO-350 and 1-D nanorods, ZnO-450, and ZnO-550, respectively.

It can be seen that dandelion-like ZnO hierarchitectures exhibit higher sensing response to ethanol compared with the 1-D nanorods. The gas sensing is correlated to the gas adsorption, desorption, and following reaction with the materials. The dandelion-like hierarchitectures have a structure highly open to the outer environment and the equally porous surface, which could provide numerous connective channels in multiscale to transport gas molecules to directly contact with the sensing material.[41] Also, the enlarged surface area of the hierarchitectures generally results in more active sites on the surface for chemical or physical interactions, increasing the reaction opportunity between gases and materials.[44] In addition, both the good crystallinity and small size are beneficial to the gas sensing response.[45,46] Therefore, a higher sensing response is obtained for dandelion-like hierarchitectures due to their porous open-ended dandelion-like structures, large surface to volume ratio, small nanoparticles size, and good crystallinity.

The results also indicate that ZnO-450 exhibits a higher sensing response than ZnO-350 and ZnO-550, which can be attributed to its better crystallinity than ZnO-350 and larger specific surface area than ZnO-550. However, considering its much higher optimal operating temperature of 370 °C than that of ZnO-350, ZnO-350 is recognized to be the ideal sensing material for detection of ethanol.

Gas sensing selectivity is one of the most important properties for the gas sensors. Figure 6 shows the gas sensing response of ZnO-350 to 50 ppm of different gases. The sensor response to ethanol is much higher than that of H_2, CO, CH_4, H_2S, NH_3, methanol, hexamethylene, and iso-propanol, but less
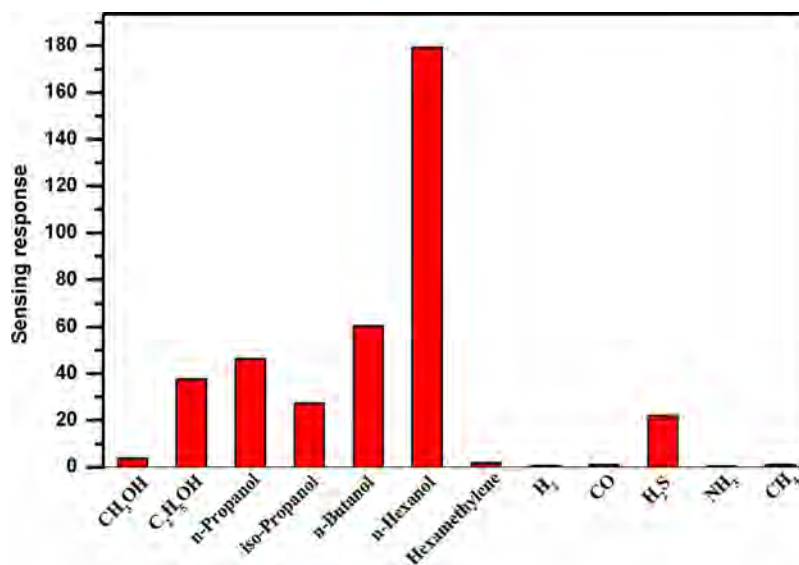

Figure 6. Gas sensing response of ZnO-350 dandelion-like hierarchitectures toward 50 ppm of different detected gases at the optimum operating temperature of 250 °C.
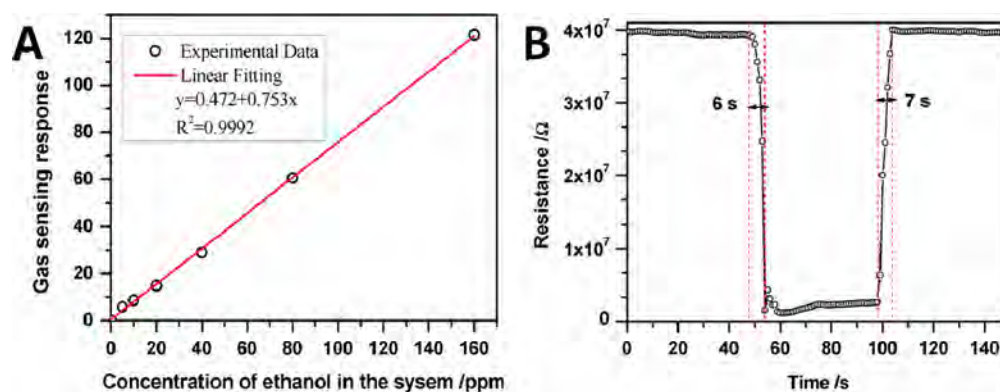
Figure 7. (A) Response curve and linear fitting curve of the sensing response of ZnO-350 to different concentration ethanol at the operating temperature of 250 °C; (B) response and recovery time of ZnO-350 to 50 ppm ethanol at the operating temperature of 250 °C.

Table 1. Comparison of the Sensing Properties toward Ethanol of the Different Material

materials	synthesis approaches	ethanol concentration (ppm)	temp (°C)	sensor response	response and recovery time (s)	ref
ZnO nanorods	hydrothermal method	50	400	6	10 and 30	16
nest-like ZnO	carbon thermal reduction	50	330	100	25 and 15	50
ZnO added MoO₃		500	300	171	75 and 75	51
flower-like ZnO nanorods	wet-chemical route	200	400	193.7	7 and 12	19
ZnO nanowires	chemical solution route	100	300	28.9		52
ZnO mesoporous architectures	solvothermal approach	100	460	26.1	6 and 38	18
Fe-doped ZnO	economical solution combustion synthesis	100	370	45	10 and 6	53
dandelion-like ZnO hierarchitectures	precipitation methods	50	250	34.5	6 and 7	this work

than that of n-propanol, n-butanol, and n-hexanol. It is well-known that oxygen species (O^{2-}, O^{-}, and O_2^{-}) are formed on the surface of the materials when ZnO is exposed to air. The oxygen species will react with the gases when the sensors are exposed to the detected gases, and the resistance of ZnO will be changed. For the ZnO material, the chemical-sensing mechanism of ethanol gas is related to its adsorption and/or oxidation of ethanol molecules,[47,48] and the reaction equation is depicted as follows:

$$C_2H_5OH + O^{-} \rightarrow CH_3CHO + H_2O + e^{-} \qquad (1)$$
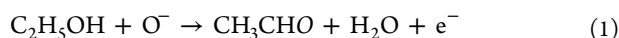
The CH_3CHO intermediate is subsequently oxidized to CO_2 and H_2O, as depicted in eq 2:

$$CH_3CHO + 5O^{-} \rightarrow 2CO_2 + 2H_2O + 5e^{-} \qquad (2)$$

The electrons donating ability is in order of $CH_3(CH_2)_5-$ > $CH_3(CH_2)_3-$ > $CH_3(CH_2)_2-$ > CH_3CH_2- > CH_3-, so the adsorption ability order is $CH_3(CH_2)_5OH$ > $CH_3(CH_2)_3OH$ > $CH_3(CH_2)_2OH$ > CH_3CH_2OH > CH_3OH. Therefore, the sequence of gas sensing response is $CH_3(CH_2)_5OH$ > $CH_3(CH_2)_3OH$ > $CH_3(CH_2)_2OH$ > CH_3CH_2OH > CH_3OH.[49] However, the adsorption of iso-propanol onto the materials will be hindered due to the steric effect, so the gas sensing response toward iso-propanol is lower than that toward ethanol. The above results indicate that the ZnO dandelion-like hierarchitectures exhibits better gas sensing selectivity to alcohols over CH_4, H_2, H_2S, NH_3, hexamethylene, and CO.

Besides, the linear response range and the response and recovery time are another two vital parameters for the sensor. Figure 7A shows the response as a function of ethanol concentration from 5 to 160 ppm for ZnO-350 at the operating temperature of 250 °C. The ZnO-350 exhibits excellent linear relationship between the sensing response and the concentration of the detected ethanol gas in the investigated range. After the linear fitting, the correlation coefficient (R^2) is 0.9992. The response and recovery time is defined as the time taken when the response value reaches 90% of the final equilibrium one. The response and recovery time of the sensor when the sensor was exposed to 50 ppm ethanol in air atmosphere is ca. 6 and 7 s as marked in the graph, respectively (Figure 7B). In comparison, Table 1 lists the gas-sensing data of the ZnO sensors to ethanol that is reported in the literature. Both of the times are much shorter than those reported in the literature as summarized in Table 1. It is worth noting that the sensor fabricated by the ZnO-350 sample in our work exhibits higher sensing response, lower operation temperature, and faster response to ethanol in comparison with others.

4. CONCLUSIONS

Dandelion-like ZnO hollow hierarchitectures assembled by nanoparticles have been synthesized by annealing a zinc complex precursor, which was produced through a facile and mild route. The nanoparticle size in the hierarchitectures enlarges from 10 to 23 nm with the annealing temperature increasing from 350 to 550 °C. The obtained ZnO hierarchitectures exhibit high sensing response, fast response and recovery, good sensing selectivity, and low optimal operating temperature toward ethanol because of high surface area and rich pore. The porous ZnO hierarchitectures synthesized in this work are one of potential gas-sensing materials for sensor applications.

ASSOCIATED CONTENT

S Supporting Information

FT-IR spectrum of the precursor, SEM, HRTEM, and XRD patterns of flower-like hierarchitectures composed by 1-D nanorods. This material is available free of charge via the Internet at http://pubs.acs.org.

AUTHOR INFORMATION

Corresponding Author
*E-mail: lidq@mail.buct.edu.cn. Fax: +86-10-64425385. Tel: +86-10-64436992.

Notes
The authors declare no competing financial interest.

ACKNOWLEDGMENTS

REFERENCES

(1) Sun, Z.; Kim, J. H.; Zhao, Y.; Bijarbooneh, F.; Malgras, V.; Lee, Y.; Kang, Y. M.; Dou, S. X. Rational Design of 3D Dendritic TiO2 Nanostructures with Favorable Architectures. *J. Am. Chem. Soc.* **2011**, *133*, 19314−19317.

(2) Joo, J. B.; Lee, I.; Dahl, M.; Moon, G. D.; Zaera, F.; Yin, Y. Controllable Synthesis of Mesoporous TiO2 Hollow Shells: Toward an Efficient Photocatalyst. *Adv. Funct. Mater.* **2013**, *23*, 4246−4254.

(3) Zhuang, Z.; Peng, Q.; Li, Y. Controlled synthesis of semiconductor nanostructures in the liquid phase. *Chem. Soc. Rev.* **2011**, *40*, 5492−5513.

(4) Zheng, Y.; Tao, X.; Hou, Q.; Wang, D.; Zhou, W.; Chen, J. Iodine-Doped ZnO Nanocrystalline Aggregates for Improved Dye-Sensitized Solar Cells. *Chem. Mater.* **2010**, *23*, 3−5.

(5) Zhang, L.; Zhang, G.; Wu, H. B.; Yu, L.; Lou, X. W. Hierarchical Tubular Structures Constructed by Carbon-Coated SnO2 Nanoplates for Highly Reversible Lithium Storage. *Adv. Mater.* **2013**, *25*, 2589−2593.

(6) Lu, Z.; Yin, Y. Colloidal nanoparticle clusters: functional materials by design. *Chem. Soc. Rev.* **2012**, *41*, 6874−6887.

(7) Wang, Y.; Jiang, X.; Xia, Y. A Solution-Phase, Precursor Route to Polycrystalline SnO2 Nanowires That Can Be Used for Gas Sensing under Ambient Conditions. *J. Am. Chem. Soc.* **2003**, *125*, 16176−16177.

(8) Wang, Y.; Lee, J. Y.; Zeng, H. C. Polycrystalline SnO2 Nanotubes Prepared via Infiltration Casting of Nanocrystallites and Their Electrochemical Application. *Chem. Mater.* **2005**, *17*, 3899−3903.

(9) Moon, G. D.; Joo, J. B.; Dahl, M.; Jung, H.; Yin, Y. Nitridation and Layered Assembly of Hollow TiO2 Shells for Electrochemical Energy Storage. *Adv. Funct. Mater.* **2014**, *24*, 848−856.

(10) Hong, Y.; Tian, C.; Jiang, B.; Wu, A.; Zhang, Q.; Tian, G.; Fu, H. Facile synthesis of sheet-like ZnO assembly composed of small ZnO particles for highly efficient photocatalysis. *J. Mater. Chem. A* **2013**, *1*, 5700−5708.

(11) Xu, J.; Chen, Y.; Chen, D.; Shen, J. Hydrothermal synthesis and gas sensing characters of ZnO nanorods. *Sens. Actuators, B* **2006**, *113*, 526−531.

(12) Sun, Y.; Fuge, G. M.; Fox, N. A.; Riley, D. J.; Ashfold, M. N. R. Synthesis of Aligned Arrays of Ultrathin ZnO Nanotubes on a Si Wafer Coated with a Thin ZnO Film. *Adv. Mater.* **2005**, *17*, 2477−2481.

(13) Ahn, M. W.; Park, K. S.; Heo, J. H.; Kim, D. W.; Choi, K. J.; Park, J. G. On-chip fabrication of ZnO-nanowire gas sensor with high gas sensitivity. *Sens. Actuators, B* **2009**, *138*, 168−173.

(14) Fan, F.; Feng, Y.; Bai, S.; Feng, J.; Chen, A.; Li, D. Synthesis and gas sensing properties to NO2 of ZnO nanoparticles. *Sens. Actuators, B* **2013**, *185*, 377−382.

(15) Bai, S.; Liu, X.; Li, D.; Chen, S.; Luo, R.; Chen, A. Synthesis of ZnO nanorods and its application in NO2 sensors. *Sens. Actuators, B* **2011**, *153*, 110−116.

(16) Chen, J.; Li, J.; Li, J.; Xiao, G.; Yang, X. Large-scale syntheses of uniform ZnO nanorods and ethanol gas sensors application. *J. Alloys Compd.* **2011**, *509*, 740−743.

(17) Li, J.; Fan, H.; Jia, X. Multilayered ZnO Nanosheets with 3D Porous Architectures: Synthesis and Gas Sensing Application. *J. Phys. Chem. C* **2010**, *114*, 14684−14691.

(18) Lu, G.; Wang, X.; Liu, J.; Qiu, S.; He, C.; Li, B.; Liu, W. One-pot synthesis and gas sensing properties of ZnO mesoporous architectures. *Sens. Actuators, B* **2013**, *184*, 85−92.

(19) Zhang, L.; Yin, Y. Large-scale synthesis of flower-like ZnO nanorods via a wet-chemical route and the defect-enhanced ethanol-sensing properties. *Sens. Actuators, B* **2013**, *183*, 110−116.

(20) Kim, H.; Choi, K.; Lee, J.; Akbar, S. A. Highly sensitive and ultra-fast responding gas sensors using self-assembled hierarchical SnO2 spheres. *Sens. Actuators, B* **2009**, *136*, 138−143.

(21) Zhang, Q.; Chou, T. P.; Russo, B.; Jenekhe, S. A.; Cao, G. Aggregation of ZnO Nanocrystallites for High Conversion Efficiency in Dye-Sensitized Solar Cells. *Angew. Chem., Int. Ed.* **2008**, *120*, 2436−2440.

(22) Narayanaswamy, A.; Xu, H.; Pradhan, N.; Kim, M.; Peng, X. Formation of Nearly Monodisperse In2O3 Nanodots and Oriented-Attached Nanoflowers: Hydrolysis and Alcoholysis vs Pyrolysis. *J. Am. Chem. Soc.* **2006**, *128*, 10310−10319.

(23) Xia, Y.; Tang, Z. Monodisperse inorganic supraparticles: formation mechanism, properties and applications. *Chem. Commun.* **2012**, *48*, 6320−6336.

(24) Choi, S. H.; Ankonina, G.; Youn, D. Y.; Oh, S. G.; Hong, J. M.; Rothschild, A.; Kim, I. D. Hollow ZnO Nanofibers Fabricated Using Electrospun Polymer Templates and Their Electronic Transport Properties. *ACS Nano* **2009**, *3*, 2623−2631.

(25) Jing, Z.; Zhan, J. Fabrication and Gas-Sensing Properties of Porous ZnO Nanoplates. *Adv. Mater.* **2008**, *20*, 4547−4551.

(26) Zhang, J.; Wang, S.; Xu, M.; Wang, Y.; Zhu, B.; Zhang, S.; Huang, W.; Wu, S. Hierarchically Porous ZnO Architectures for Gas Sensor Application. *Cryst. Growth Des.* **2009**, *9*, 3532−3537.

(27) Duan, X.; Wang, G.; Wang, H.; Wang, Y.; Shen, C.; Cai, W. Orientable pore-size-distribution of ZnO nanostructures and their superior photocatalytic activity. *CrystEngComm* **2010**, *12*, 2821−2825.

(28) Sin, J. C.; Lam, S. M.; Lee, K. T.; Mohamed, A. R. Fabrication of erbium-doped spherical-like ZnO hierarchical nanostructures with enhanced visible light-driven photocatalytic activity. *Mater. Lett.* **2013**, *91*, 1−4.

(29) Song, R. Q.; Xu, A. W.; Deng, B.; Li, Q.; Chen, G. Y. From Layered Basic Zinc Acetate Nanobelts to Hierarchical Zinc Oxide Nanostructures and Porous Zinc Oxide Nanobelts. *Adv. Funct. Mater.* **2007**, *17*, 296−306.

(30) Ku, C. H.; Yang, H. H.; Chen, G. R.; Wu, J. J. Wet-Chemical Route to ZnO Nanowire-Layered Basic Zinc Acetate/ZnO Nanoparticle Composite Film. *Cryst. Growth Des.* **2007**, *8*, 283−290.

(31) Qi, Q.; Zhao, J.; Xuan, R.; Wang, P.; Feng, L.; Zhou, L.; Wang, D.; Li, G. Sensitive ethanol sensors fabricated from p-type La0.7Sr0.3FeO3 nanoparticles and n-type SnO2 nanofibers. *Sens. Actuators, B* **2014**, *191*, 659−665.

(32) Liu, L.; Liu, C.; Li, S.; Wang, L.; Shan, H.; Zhang, X.; Guan, H.; Liu, Z. Honeycombed SnO2 with ultra sensitive properties to H2. *Sens. Actuators, B* **2013**, *177*, 893−897.

(33) Cursino, A. C. T.; Gardolinski, J. E. F. C.; Wypych, F. Intercalation of anionic organic ultraviolet ray absorbers into layered zinc hydroxide nitrate. *J. Colloid Interface Sci.* **2010**, *347*, 49−55.

(34) Su, B.; Li, M.; Shi, Z.; Lu, Q. From Superhydrophilic to Superhydrophobic: Controlling Wettability of Hydroxide Zinc Carbonate Film on Zinc Plates. *Langmuir* **2009**, *25*, 3640−3645.

(35) Li, Z.; Zhao, Q.; Fan, W.; Zhan, J. Porous SnO2 nanospheres as sensitive gas sensors for volatile organic compounds detection. *Nanoscale* **2011**, *3*, 1646−1652.

(36) Li, C. C.; Yin, X. M.; Wang, T. H.; Zeng, H. C. Morphogenesis of Highly Uniform $CoCO_3$ Submicrometer Crystals and Their Conversion to Mesoporous Co_3O_4 for Gas-Sensing Applications. *Chem. Mater.* **2009**, *21*, 4984−4992.

(37) Lai, X.; Wang, D.; Han, N.; Du, J.; Li, J.; Xing, C.; Chen, Y.; Li, X. Ordered Arrays of Bead-Chain-like In_2O_3 Nanorods and Their Enhanced Sensing Performance for Formaldehyde. *Chem. Mater.* **2010**, *22*, 3033−3042.

(38) Chiang, Y. J.; Pan, F. M. PdO Nanoflake Thin Films for CO Gas Sensing at Low Temperatures. *J. Phys. Chem. C* **2013**, *117*, 15593−15601.

(39) Bai, S.; Zhang, K.; Luo, R.; Li, D.; Chen, A.; Liu, C. C. Low-temperature hydrothermal synthesis of WO_3 nanorods and their sensing properties for NO_2. *J. Mater. Chem.* **2012**, *22*, 12643−12650.

(40) Bai, S.; Hu, J.; Li, D.; Luo, R.; Chen, A.; Liu, C. C. Quantum-sized ZnO nanoparticles: Synthesis, characterization and sensing properties for NO_2. *J. Mater. Chem.* **2011**, *21*, 12288−12294.

(41) Song, F.; Su, H.; Chen, J.; Moon, W. J.; Lau, W. M.; Zhang, D. 3D hierarchical porous SnO_2 derived from self-assembled biological systems for superior gas sensing application. *J. Mater. Chem.* **2012**, *22*, 1121−1126.

(42) Qin, Y.; Zhang, F.; Chen, Y.; Zhou, Y.; Li, J.; Zhu, A.; Luo, Y.; Tian, Y.; Yang, J. Hierarchically Porous CuO Hollow Spheres Fabricated via a One-Pot Template-Free Method for High-Performance Gas Sensors. *J. Phys. Chem. C* **2012**, *116*, 11994−12000.

(43) Zhang, F.; Zhu, A.; Luo, Y.; Tian, Y.; Yang, J.; Qin, Y. CuO Nanosheets for Sensitive and Selective Determination of H_2S with High Recovery Ability. *J. Phys. Chem. C* **2010**, *114*, 19214−19219.

(44) Shi, Y.; Wang, M.; Hong, C.; Yang, Z.; Deng, J.; Song, X.; Wang, L.; Shao, J.; Liu, H.; Ding, Y. Multi-junction joints network self-assembled with converging ZnO nanowires as multi-barrier gas sensor. *Sens. Actuators, B* **2013**, *177*, 1027−1034.

(45) Katoch, A.; Sun, G.; Choi, S.; Byun, J.; Kim, S. Competitive influence of grain size and crystallinity on gas sensing performances of ZnO nanofibers. *Sens. Actuators, B* **2013**, *185*, 411−416.

(46) Choi, Y. H.; Kim, D. H.; Han, H. S.; Shin, S.; Hong, S. H.; Hong, K. S. Direct Printing Synthesis of Self-Organized Copper Oxide Hollow Spheres on a Substrate Using Copper(II) Complex Ink: Gas Sensing and Photoelectrochemical Properties. *Langmuir* **2014**, *30*, 700−709.

(47) Hamedani, N. F.; Mahjoub, A. R.; khodadadi, A. A.; Mortazavi, Y. CeO_2 doped ZnO flower-like nanostructure sensor selective to ethanol in presence of CO and CH_4. *Sens. Actuators, B* **2012**, *169*, 67−73.

(48) Khoang, N. D.; Trung, D. D.; Van Duy, N.; Hoa, N. D.; Van Hieu, N. Design of SnO_2/ZnO hierarchical nanostructures for enhanced ethanol gas-sensing performance. *Sens. Actuators, B* **2012**, *174*, 594−601.

(49) Kaneti, Y. V.; Yue, J.; Jiang, X.; Yu, A. Controllable Synthesis of ZnO Nanoflakes with Exposed ($10\bar{1}0$) for Enhanced Gas Sensing Performance. *J. Phys. Chem. C* **2013**, *117*, 13153−13162.

(50) Qin, N.; Wang, X.; Xiang, Q.; Xu, J. A biomimetic nest-like ZnO: Controllable synthesis and enhanced ethanol response. *Sens. Actuators, B* **2014**, *191*, 770−778.

(51) Illyaskutty, N.; Kohler, H.; Trautmann, T.; Schwotzer, M.; Pillai, V. P. M. Enhanced ethanol sensing response from nanostructured MoO_3:ZnO thin films and their mechanism of sensing. *J. Mater. Chem. C* **2013**, *1*, 3976−3984.

(52) Huang, J.; Ren, H.; Sun, P.; Gu, C.; Sun, Y.; Liu, J. Facile synthesis of porous ZnO nanowires consisting of ordered nanocrystallites and their enhanced gas-sensing property. *Sens. Actuators, B* **2013**, *188*, 249−256.

(53) Cai, Y.; Fan, H.; Xu, M.; Li, Q.; Long, C. Fast economical synthesis of Fe-doped ZnO hierarchical nanostructures and their high gas-sensing performance. *CrystEngComm* **2013**, *15*, 7339−7345.

12743

dx.doi.org/10.1021/ie501825t | *Ind. Eng. Chem. Res.* 2014, 53, 12737−12743